

# Magnetic fluctuations driven by quantum geometry

Makoto Shimizu,<sup>1, 2,\*</sup> Chang-guen Oh,<sup>1, 3, †</sup> and Youichi Yanase<sup>2</sup>

<sup>1</sup>These authors contributed equally to this work.

<sup>2</sup>Department of Physics, Graduate School of Science, Kyoto University, Kyoto 606-8502, Japan

<sup>3</sup>Department of Applied Physics, The University of Tokyo, Tokyo 113-8656, Japan

(Dated: February 17, 2026)

Using quantum distance, magnetic susceptibility in the non-interacting limit can be rigorously split into two contributions: one arising solely from band dispersion, while the other stems from quantum geometric contributions. In this Letter, we apply this decomposition to two materials, LaFeAsO and  $\text{Pb}_9\text{Cu}(\text{PO}_4)_6\text{O}$ , and demonstrate that their dominant magnetic fluctuations originate from the geometric contribution. In LaFeAsO, stripe-type antiferromagnetic fluctuations arise primarily from quantum geometry, while in  $\text{Pb}_9\text{Cu}(\text{PO}_4)_6\text{O}$  the geometric term suppresses antiferromagnetic fluctuations and stabilizes ferromagnetic fluctuations. Our findings highlight the essential role of quantum geometry in governing magnetic fluctuations in multi-band systems, and provide a unique and quantitative framework to disentangle band-structure and wavefunction-geometry effects that have often been discussed collectively as multi-orbital effects.

*Introduction.*—In spin fluctuation theory, antiferromagnetic fluctuations are traditionally explained by Fermi surface nesting [1–3]. In its original form, nesting refers solely to the property of energy dispersion, and the nesting vector  $\mathbf{Q}$  is chosen to maximize the Lindhard function. This description is exact in systems without inter-band hybridization, where the irreducible susceptibility is equal to the Lindhard function. However, in multi-band systems, this understanding must be extended to incorporate the overlap of Wannier functions [4–7]. This is because the irreducible susceptibility in multi-band systems is not simply proportional to the Lindhard function and affected by matrix elements involving wavefunctions. Consequently, both Fermi surface nesting and orbital overlap must be considered to understand spin fluctuations appropriately. Nesting between orbitals with negligible overlap does not enhance spin susceptibility, even if nesting appears favorable based on band dispersion alone.

The overlap of Bloch states is naturally captured by quantum geometry. In particular, the Hilbert-Schmidt quantum distance [8, 9] measures the difference of Bloch wave functions. Together with the quantum-geometric tensor [8–10], the geometric nature of Bloch states has been shown to influence a broad spectrum of electronic phenomena, such as topological properties of materials [11, 12], electromagnetic responses in superconductors [13–16], anomalous Landau-level spreading [17, 18], electronic polarizability [19, 20], transport properties in bilayer graphene [21, 22], thermoelectric transport via disorder-mediated scattering [23], optical conductivity [24–29], and bulk-interface correspondence in singular flat-band systems [30, 31]. Recently, it has been shown that a necessary condition for ferromagnetic ordering can be expressed in terms of the quantum metric [32], forging a deep connection between magnetism and quantum

geometry [32–38]. By contrast, antiferromagnetic fluctuations do not admit a formulation purely in the metric; instead, they emerge naturally through the quantum-distance contribution to the non-interacting susceptibility [32]. This insight enables a decomposition of the irreducible susceptibility into a “band” term, dependent only on energy dispersion, and a “geometric” term, capturing wavefunction-overlap effects.

In multi-band systems, crystal structures and chemical compositions strongly shape the electronic structure and, consequently, the magnetic fluctuations. Understanding magnetism in such systems therefore requires investigations based on realistic electronic structures obtained from first-principles calculations [5–7, 39]. While quantum geometric effects on magnetism have been clarified at a formal level, their relevance in realistic material-specific models has remained largely unexplored. In particular, it is an open question how the decomposition of the irreducible susceptibility into band and geometric contributions emerges in effective models constructed from first-principles calculations. Addressing this issue is essential for assessing the physical significance of quantum geometry beyond idealized model studies.

In this Letter, we investigate quantum geometric effects in realistic materials. Starting from first-principles calculations within density functional theory (DFT), we construct effective tight-binding models and evaluate the irreducible susceptibility, which is equivalent to the magnetic susceptibility in the non-interacting limit. We then decompose the susceptibility into the band and geometric contributions, following Refs. [32, 37]. We demonstrate that in LaFeAsO and  $\text{Pb}_9\text{Cu}(\text{PO}_4)_6\text{O}$ , the dominant magnetic fluctuations arise from the geometric term. LaFeAsO is a parent compound of iron-based superconductors, where stripe-type antiferromagnetic fluctuations at  $\mathbf{Q} = (\pi, 0)$  play a key role in superconductivity [5, 39, 40]. While the mechanism of the antiferromagnetic fluctuations has been discussed in terms of Fermi-surface nesting [5, 39], we revisit it from the perspective of quantum geometry. The second material,

\* [shimizu.makoto.5c@kyoto-u.ac.jp](mailto:shimizu.makoto.5c@kyoto-u.ac.jp)

† [cg.oh.0404@gmail.com](mailto:cg.oh.0404@gmail.com)

Pb9Cu(PO4)6O, has attracted attention for the claim of room-temperature superconductivity, but this claim has largely been refuted. Nevertheless, early theoretical works [41, 42] pointed to its intriguing quantum geometric properties, such as a large Berry curvature and the presence of Weyl points. The impact of these geometric features on the magnetic response, however, has not yet been explored. Experimental [43–45] and theoretical [46–48] studies have suggested ferromagnetic fluctuations in this material. We show that, in both materials, the dominant magnetic fluctuations are induced by the contribution which we refer to the geometric term.

*Formalism.*—We consider a tight-binding model described by the Hamiltonian

$$H_0 = \sum_{ij} \sum_{lm} \sum_{\sigma} t_{ij}^{lm} c_{il\sigma}^{\dagger} c_{jm\sigma}, \quad (1)$$

where  $i$  and  $j$  label lattice sites,  $l$  and  $m$  are orbital indices, and  $\sigma$  denotes the spin. In momentum space, the matrix representation of the Hamiltonian is denoted by  $H_0(\mathbf{k})$ , and its eigenvalue equation reads  $H_0(\mathbf{k}) |u_{\lambda}(\mathbf{k})\rangle = E_{\lambda}(\mathbf{k}) |u_{\lambda}(\mathbf{k})\rangle$ . Here,  $E_{\lambda}(\mathbf{k})$  is the energy dispersion, and  $|u_{\lambda}(\mathbf{k})\rangle$  is the corresponding Bloch wavefunction. The index  $\lambda$  labels bands.

In this work, we focus on the static irreducible susceptibility, which we decompose into band and geometric contributions [32, 37]:

$$\chi^0(\mathbf{q}) = \chi_{\text{band}}^0(\mathbf{q}) + \chi_{\text{geom}}^0(\mathbf{q}). \quad (2)$$

The two terms are given explicitly as

$$\chi_{\text{geom}}^0(\mathbf{q}) = \sum_{\mathbf{k}} \sum_{\lambda\lambda'} [1 - d_{\lambda\lambda'}^2(\mathbf{k}, \mathbf{k} + \mathbf{q}) - \delta_{\lambda\lambda'}] F_{\lambda\lambda'}(\mathbf{k}, \mathbf{q}), \quad (3)$$

$$\chi_{\text{band}}^0(\mathbf{q}) = \sum_{\mathbf{k}} \sum_{\lambda\lambda'} \delta_{\lambda\lambda'} F_{\lambda\lambda'}(\mathbf{k}, \mathbf{q}), \quad (4)$$

where  $F_{\lambda\lambda'}(\mathbf{k}, \mathbf{q})$  is the Lindhard function defined as

$$F_{\lambda\lambda'}(\mathbf{k}, \mathbf{q}) = -\frac{f(E_{\lambda}(\mathbf{k})) - f(E_{\lambda'}(\mathbf{k} + \mathbf{q}))}{E_{\lambda}(\mathbf{k}) - E_{\lambda'}(\mathbf{k} + \mathbf{q})}, \quad (5)$$

with  $f(E)$  being the Fermi-Dirac distribution function. The quantity  $d_{\lambda\lambda'}(\mathbf{k}, \mathbf{k}')$  represents the quantum distance between the Bloch states  $|u_{\lambda}(\mathbf{k})\rangle$  and  $|u_{\lambda'}(\mathbf{k}')\rangle$ , given by

$$d_{\lambda\lambda'}^2(\mathbf{k}, \mathbf{k}') = 1 - |\langle u_{\lambda}(\mathbf{k}) | u_{\lambda'}(\mathbf{k}') \rangle|^2. \quad (6)$$

In systems with trivial band geometry—i.e., in the absence of inter-band hybridization such that  $\langle u_{\lambda}(\mathbf{k}) | u_{\lambda'}(\mathbf{k}') \rangle = \delta_{\lambda\lambda'}$ —the quantum distance is simplified to  $d_{\lambda\lambda'}^2(\mathbf{k}, \mathbf{k}') = 1 - \delta_{\lambda\lambda'}$ . Consequently, the geometric contribution vanishes, and the irreducible susceptibility reduces to the band term:  $\chi^0(\mathbf{q}) = \chi_{\text{band}}^0(\mathbf{q})$ .

*Antiferromagnetic fluctuations induced by quantum geometry.*—To obtain the electronic structure of LaFeAsO, we adopt crystallographic parameters from

Ref. [49] and perform all-electron DFT calculations. The calculations are carried out using the full-potential local orbital (FPLO) basis set [50], the generalized gradient approximation (GGA) exchange-correlation functional [51] and a  $24 \times 24 \times 24$   $k$ -mesh.

We construct a tight-binding model comprising all ten Fe  $3d$  orbitals using symmetry-conserving projected Wannier functions implemented in FPLO [52]. Using the glide-reflection unfolding technique [53], we reduce the ten-band model to an effective five-band model. The resulting band structure and the Fermi surface of the unfolded model are shown in Fig. 1. Because interlayer hopping is negligibly small, the band dispersion is nearly independent of  $k_z$ , and the Fermi surface is almost cylindrical along the  $k_z$  direction. Therefore, in the following analysis, we neglect the  $k_z$  dependence of the electronic structure. Near the  $\Gamma$  point [ $\mathbf{k} = (0, 0)$ ], two hole pockets are formed mainly by the  $3d_{xz/yz}$  orbitals. Around the  $X$  point [ $\mathbf{k} = (\frac{1}{2}, 0)$ ], an electron pocket appears with dominant contributions from the  $3d_{xy}$  and  $3d_{xz/yz}$  orbitals. Around the  $M$  point [ $\mathbf{k} = (\frac{1}{2}, \frac{1}{2})$ ], another hole pocket arises from the  $3d_{xy}$  orbital. This band structure is consistent with earlier studies of LaFeAsO [5].

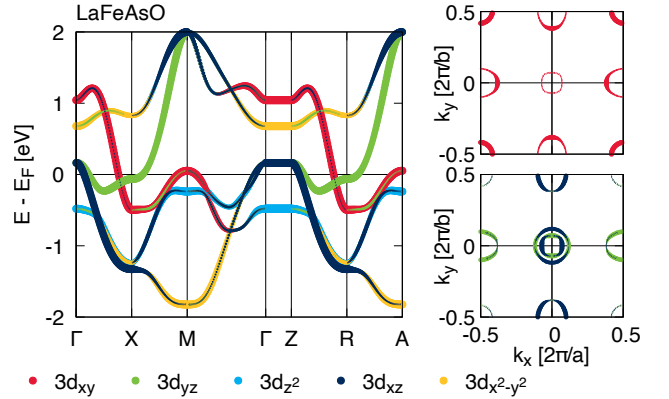


FIG. 1. Band structure (left) and Fermi surface (right) of LaFeAsO. Colors show the orbital weights of Fe  $3d_{xy}$  (red),  $3d_{yz}$  (green),  $3d_{z2}$  (blue),  $3d_{xz}$  (navy) and  $3d_{x^2-y^2}$  (yellow).

We compute the static irreducible susceptibility  $\chi^0(\mathbf{q})$ , its band contribution  $\chi_{\text{band}}^0(\mathbf{q})$  and geometric contribution  $\chi_{\text{geom}}^0(\mathbf{q})$  on a  $64 \times 64 \times 1$   $q$ -mesh at  $T = 116$  K. As shown in Fig. 2 (a), the total susceptibility exhibits prominent peaks at  $\mathbf{Q} = (\frac{1}{2}, 0)$  and symmetry-related points. Decomposing  $\chi^0(\mathbf{q})$  into the band and geometric terms, we identify their respective contributions [Figs. 2 (b) and 2 (c)]. The band contribution,  $\chi_{\text{band}}^0(\mathbf{q})$  [Fig. 2 (b)], shows only broad features and does not favor the ordering at  $\mathbf{Q}$ . In stark contrast, the geometric contribution,  $\chi_{\text{geom}}^0(\mathbf{q})$  [Fig. 2 (c)], exhibits dominant peaks exactly at these antiferromagnetic wave vectors. Therefore, we conclude that the stripe-type antiferromagnetic instability in LaFeAsO is decisively driven by the quantum geometry of the Bloch states.

*Ferromagnetic fluctuations induced by quantum*

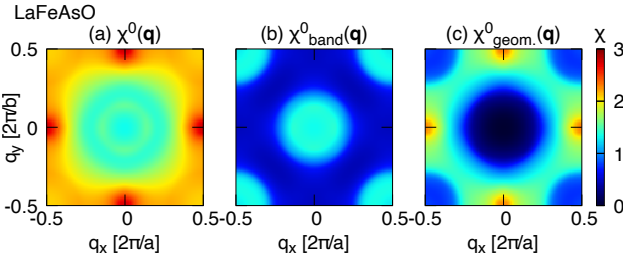


FIG. 2. (a) The static spin susceptibility, (b) the band term and (c) the geometric term for LaFeAsO at  $T = 116$  K.

*geometry.*—We construct the crystal structure of  $\text{Pb}_9\text{Cu}(\text{PO}_4)_6\text{O}$  following the method in Ref. [46]. The process starts from the structure of  $\text{Pb}_{10}(\text{PO}_4)_6\text{O}$  determined by Krivovichev and Burns [54], which belongs to the  $P63/m$  (No. 176) space group and has a partially occupied (one-quarter) O(4) site. To simplify the model, we select one of four symmetry-equivalent O(4) sites, thereby reducing the symmetry to  $P3$  (No. 143). According to Ref. [55], substitution of Cu at the Pb(2) site is energetically favorable. We thus replace one of the four Pb atoms with a Cu atom and relax the internal atomic positions. Using experimentally determined lattice constants [56], we perform all-electron DFT calculations with the FPLO basis set [50], the GGA exchange-correlation functional [51], and a  $12 \times 12 \times 12$   $k$ -mesh.

A four-band tight-binding model is constructed from projected Wannier functions [52], incorporating the Cu  $3d_{xz}$ ,  $3d_{yz}$  and O  $2p_x$ ,  $2p_y$  orbitals. The resulting band structure and Fermi surface are shown in Fig. 3. For stoichiometric  $\text{Pb}_9\text{Cu}(\text{PO}_4)_6\text{O}$ , the total electron filling is  $n = 7$ . To explore ferromagnetism in the electron-doped region, as suggested by the fluctuation exchange approximation [46], we set the chemical potential to  $\mu = 10$  meV, corresponding to an electron doping level of  $\Delta n \approx 0.4$ .

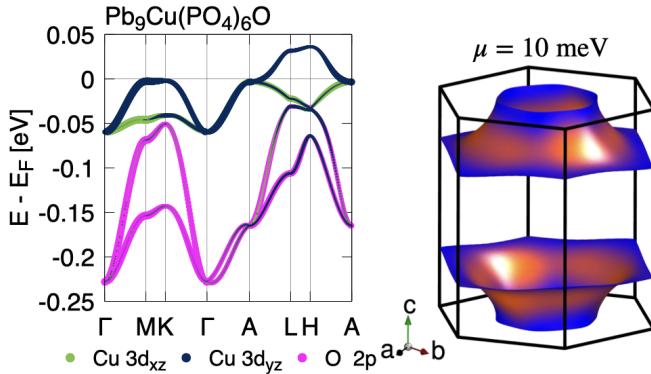


FIG. 3. Band structure (left) and Fermi surface (right) of  $\text{Pb}_9\text{Cu}(\text{PO}_4)_6\text{O}$ . The Fermi surface is displayed for the chemical potential,  $\mu = 10$  meV. Orange (blue) indicates high (low) Fermi velocity as determined by the FPLO calculation.

We calculate the static spin susceptibility  $\chi^0$ , its band

part  $\chi^0_{\text{band}}$ , and geometric part  $\chi^0_{\text{geom}}$  on a  $64 \times 64 \times 32$   $k$ -mesh at  $T = 116$  K, considering only the spin of Cu  $3d$  orbitals. The total static susceptibility [Figs. 4 (a1)–(a3)] exhibits a peak at  $\mathbf{Q}_\Gamma = (0, 0, 0)$ , indicating a ferromagnetic fluctuation. Upon decomposing  $\chi^0$ , we find that the band term [Figs. 4 (b1)–(b3)] shows peaks at  $\mathbf{Q}_H = (\frac{1}{2}, \frac{1}{2}, \frac{1}{2})$ , which would favor antiferromagnetic fluctuations if the geometric term were absent. However, the geometric contribution,  $\chi^0_{\text{geom}}(\mathbf{q})$  [Figs. 4 (c1)–(c3)], is negative for all  $\mathbf{q}$ , with particularly large magnitude at  $\mathbf{Q}_H$ , thereby suppressing the antiferromagnetic tendency. As a result, the total susceptibility  $\chi^0(\mathbf{q})$  at  $\mathbf{Q}_H$  is diminished, leaving the ferromagnetic fluctuation at  $\mathbf{Q}_\Gamma$  as the leading instability. We thus conclude that quantum geometry stabilizes ferromagnetism in electron-doped  $\text{Pb}_9\text{Cu}(\text{PO}_4)_6\text{O}$  by actively suppressing the competing antiferromagnetic order favored by the band structure.

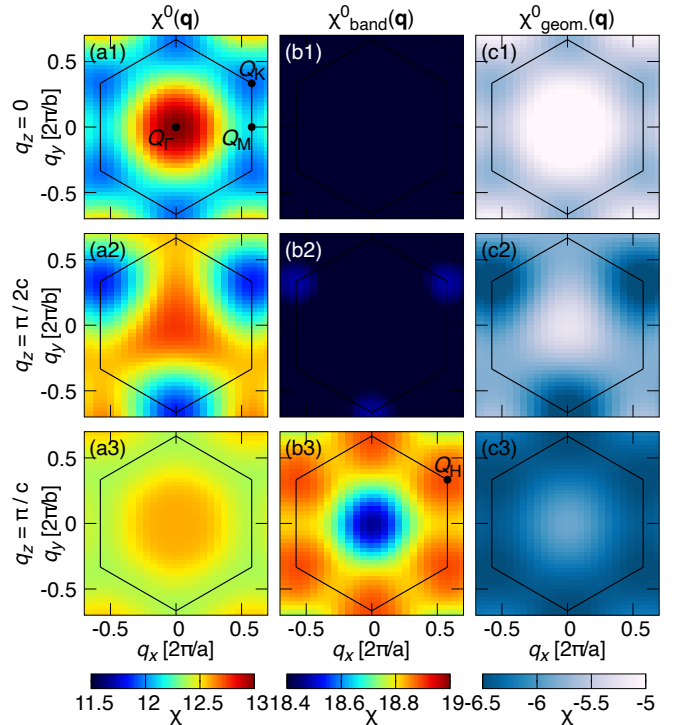


FIG. 4. Static irreducible susceptibility of electron-doped  $\text{Pb}_9\text{Cu}(\text{PO}_4)_6\text{O}$  ( $\mu = 10$  meV) at  $T = 116$  K. Total susceptibility  $\chi^0$  (left), the band term  $\chi^0_{\text{band}}$  (middle) and the geometric term  $\chi^0_{\text{geom}}$  (right) are plotted. Cuts through  $q_z = 0$  (top),  $q_z = \pi/2c$  (middle) and  $q_z = \pi/c$  (bottom) are shown.

*Discussion.*—We have demonstrated that magnetic fluctuations in two realistic materials are predominantly governed by quantum geometry, but through strikingly different mechanisms. This distinction originates from the sign of the geometric contribution,  $\chi^0_{\text{geom}}$ : In LaFeAsO, it is positive and enhances antiferromagnetic fluctuations at  $\mathbf{Q} = (1/2, 0)$ . In contrast, in electron-doped  $\text{Pb}_9\text{Cu}(\text{PO}_4)_6\text{O}$ , it is negative and suppresses the

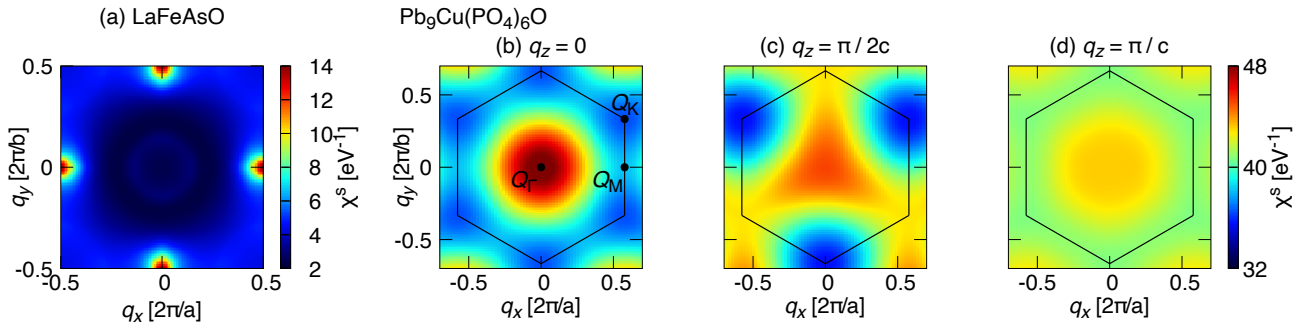


FIG. 5. Static spin susceptibility  $\chi^s(\mathbf{q})$  calculated within RPA. (a) LaFeAsO for onsite Coulomb interaction parameters  $U = 0.8$  eV,  $V = U/2$ , and  $J = J' = U/4$  at  $T = 116$  K, showing a pronounced peak at  $\mathbf{Q} = (\frac{1}{2}, 0)$ . (b-d)  $\text{Pb}_9\text{Cu}(\text{PO}_4)_6\text{O}$  ( $\mu = 10$  meV) for  $U = 100$  meV,  $V = U/2$ , and  $J = J' = U/4$  at  $T = 116$  K, showing  $\chi^s(\mathbf{q})$  for  $q_z = 0$ ,  $\pi/2c$ , and  $\pi/c$ , respectively. A ferromagnetic peak at  $\mathbf{Q} = (0, 0, 0)$  is enhanced, while antiferromagnetic fluctuations are suppressed.

antiferromagnetic fluctuations favored by the band structure, allowing ferromagnetic fluctuations at  $\mathbf{Q} = (0, 0, 0)$  to become dominant.

A crucial question is whether this geometrically-driven magnetic tendency persists in the presence of electron-electron interactions. To address this, we employ the random phase approximation (RPA) and calculate spin susceptibility in interacting systems. As confirmed by our results (Fig. 5), the peak positions of the magnetic susceptibility remain unchanged upon including electron-electron interactions. In LaFeAsO, the peak at  $\mathbf{Q} = (\frac{1}{2}, 0)$  is enhanced by interactions, consistent with previous studies [5]. In  $\text{Pb}_9\text{Cu}(\text{PO}_4)_6\text{O}$ , the ferromagnetic peak at  $\mathbf{Q} = (0, 0, 0)$  is likewise intensified, in agreement with Ref. [46]. These results indicate that the geometric origin of magnetic fluctuations persists at least in the weak-coupling regime. See the calculation details in the Supplemental Materials [57].

The geometric origin of the antiferromagnetic fluctuations observed in LaFeAsO may be common in other iron-based superconductors, which share similar Fermi surfaces and orbital characters. Quantum geometry thus emerges as a key factor in controlling magnetic responses across the family of iron-based superconductors. For example, some compounds in this class display other types of antiferromagnetic fluctuations with  $\mathbf{Q} = (1/2, 1/2)$  [58] and  $\mathbf{Q} = (1/4, 1/4)$  [59, 60] in addition to the stripe-type fluctuations at  $\mathbf{Q} = (1/2, 0)$ . The interplay between these magnetic fluctuations gives rise to a variety of superconducting gap symmetries, including  $d_{x^2-y^2}$ -wave, nodal  $s_{\pm}$ -wave, and nodeless  $s_{\pm}$ -wave states [6]. Applying the band-geometry decomposition to this broader class of materials could elucidate how wavefunction geometry governs the competition between distinct magnetic instabilities and the resulting superconducting gap structures.

In the case of  $\text{Pb}_9\text{Cu}(\text{PO}_4)_6\text{O}$ , the ferromagnetic fluctuation is revealed to originate from quantum geometry. While Ref. [46] proposed that ferromagnetism might arise

from the energy dispersion along the  $k_z$  direction, our analysis indicates that the dispersion alone is insufficient. The geometric term is indispensable for stabilizing the ferromagnetic response.

In summary, we have demonstrated that quantum geometry, quantified via the quantum distance, plays a decisive role in driving both antiferromagnetic and ferromagnetic fluctuations in realistic materials. By applying the band-geometric decomposition of susceptibility to first-principles-based tight-binding models, we have revealed that the dominant magnetic fluctuations in LaFeAsO and  $\text{Pb}_9\text{Cu}(\text{PO}_4)_6\text{O}$  originate from the geometric contribution. Our results highlight the crucial importance of quantum geometry in understanding magnetism in multi-band systems and suggest that this framework can be broadly extended to other correlated electron systems.

The present framework opens a route to systematically classify magnetic fluctuations in multi-band systems by disentangling band-dispersion and wavefunction-geometry contributions in a unique and quantitative manner. While the importance of orbital matrix elements beyond simple Fermi-surface nesting has been recognized in various contexts, the band-geometric decomposition based on the quantum distance provides a unified and quantitative framework to organize such effects. Applying this approach to a broad range of materials will facilitate the identification of compounds in which magnetism is predominantly controlled by wavefunction geometry, thereby providing a practical guideline for exploring magnetic and superconducting materials.

M. S. is supported by ISHIZUE 2025 of Kyoto University. Y. Y. is supported by JSPS KAKENHI (Grant Numbers JP22H01181, JP22H04933, JP23K17353, JP23K22452, JP24K21530, JP24H00007, JP25H01249). C. O. was supported by JSPS KAKENHI Grant Number JP25KF0186. The computation in this work has been done using the facilities of the Supercomputer Center, the Institute for Solid State Physics, the University of Tokyo (ISSPkyodo-SC-2025-Ca-0062).

---

[1] P. A. Fedders and P. C. Martin, Itinerant Antiferromagnetism, *Phys. Rev.* **143**, 245 (1966).

[2] A. Shibatani, K. Motizuki, and T. Nagamiya, Spin Density Wave in Chromium and Its Alloys, *Phys. Rev.* **177**, 984 (1969).

[3] T. M. Rice, Band-Structure Effects in Itinerant Antiferromagnetism, *Phys. Rev. B* **2**, 3619 (1970).

[4] Y. Yanase, M. Mochizuki, and M. Ogata, Multi-orbital Analysis on the Superconductivity in  $\text{Na}_x\text{CoO}_2\text{-}y\text{H}_2\text{O}$ , *Journal of the Physical Society of Japan* **74**, 430 (2005).

[5] K. Kuroki, S. Onari, R. Arita, H. Usui, Y. Tanaka, H. Kontani, and H. Aoki, Unconventional Pairing Originating from the Disconnected Fermi Surfaces of Superconducting  $\text{LaFeAsO}_{1-x}\text{F}_x$ , *Phys. Rev. Lett.* **101**, 087004 (2008).

[6] K. Kuroki, H. Usui, S. Onari, R. Arita, and H. Aoki, Pnictogen height as a possible switch between high- $T_c$  nodeless and low- $T_c$  nodal pairings in the iron-based superconductors, *Phys. Rev. B* **79**, 224511 (2009).

[7] M. Shimizu, N. Takemori, D. Guterding, and H. O. Jeschke, Two-Dome Superconductivity in FeS Induced by a Lifshitz Transition, *Phys. Rev. Lett.* **121**, 137001 (2018).

[8] J. P. Provost and G. Vallee, Riemannian structure on manifolds of quantum states, *Communications in Mathematical Physics* **76**, 289 (1980).

[9] A. Shapere and F. Wilczek, *Geometric Phases in Physics*, Vol. 5 (World scientific, 1989).

[10] Y.-Q. Ma, S. Chen, H. Fan, and W.-M. Liu, Abelian and non-Abelian quantum geometric tensor, *Phys. Rev. B* **81**, 245129 (2010).

[11] N. Nagaosa, J. Sinova, S. Onoda, A. H. MacDonald, and N. P. Ong, Anomalous Hall effect, *Rev. Mod. Phys.* **82**, 1539 (2010).

[12] D. Xiao, M.-C. Chang, and Q. Niu, Berry phase effects on electronic properties, *Rev. Mod. Phys.* **82**, 1959 (2010).

[13] S. Peotta and P. Törmä, Superfluidity in topologically nontrivial flat bands, *Nat. Commun.* **6**, 8944 (2015).

[14] P. Törmä, S. Peotta, and B. A. Bernevig, Superconductivity, superfluidity and quantum geometry in twisted multilayer systems, *Nat. Rev. Phys.* **4**, 528 (2022).

[15] H. Tanaka, H. Watanabe, and Y. Yanase, Nonlinear optical response in superconductors in magnetic field: Quantum geometry and topological superconductivity, *Phys. Rev. B* **110**, 014520 (2024).

[16] C.-g. Oh, H. Watanabe, and N. Tsuji, Role of quantum geometry in the competition between higgs mode and quasiparticles in third-harmonic generation of superconductors, arXiv preprint arXiv:2512.01200 (2025).

[17] J.-W. Rhim, K. Kim, and B.-J. Yang, Quantum distance and anomalous Landau levels of flat bands, *Nature* **584**, 59 (2020).

[18] Y. Hwang, J.-W. Rhim, and B.-J. Yang, Geometric characterization of anomalous landau levels of isolated flat bands, *Nature communications* **12**, 6433 (2021).

[19] R. Resta, Polarization fluctuations in insulators and metals: New and old theories merge, *Phys. Rev. Lett.* **96**, 137601 (2006).

[20] N. Verma, D. Guerci, and R. Queiroz, Geometric stiffness in interlayer exciton condensates, *Phys. Rev. Lett.* **132**, 236001 (2024).

[21] C.-g. Oh, J.-W. Rhim, and B.-J. Yang, Revisiting the magnetic responses of bilayer graphene from the perspective of quantum distance, *Phys. Rev. B* **110**, 155412 (2024).

[22] S.-H. Han, J.-W. Rhim, and C.-g. Oh, Klein tunneling in quantum geometric semimetals, arXiv preprint arXiv:2601.12797 (2026).

[23] C.-g. Oh, K. W. Kim, and J.-W. Rhim, Thermoelectric transport driven by the Hilbert–Schmidt distance, *Adv. Sci.* **11**, 2411313 (2024).

[24] P. Bhalla, K. Das, D. Culcer, and A. Agarwal, Resonant second-harmonic generation as a probe of quantum geometry, *Phys. Rev. Lett.* **129**, 227401 (2022).

[25] B. Ghosh, Y. Onishi, S.-Y. Xu, H. Lin, L. Fu, and A. Bansil, Probing quantum geometry through optical conductivity and magnetic circular dichroism, *Sci. Adv.* **10**, eado1761 (2024).

[26] M. Ezawa, Analytic approach to quantum metric and optical conductivity in Dirac models with parabolic mass in arbitrary dimensions, *Phys. Rev. B* **110**, 195437 (2024).

[27] J. Ahn, G.-Y. Guo, N. Nagaosa, and A. Vishwanath, Riemannian geometry of resonant optical responses, *Nat. Phys.* **18**, 290 (2022).

[28] C.-g. Oh, S.-W. Kim, K. W. Kim, B. Monserrat, and J.-W. Rhim, Universal optical conductivity from quantum geometry in quadratic band-touching semimetals, arXiv preprint arXiv:2503.18372 (2025).

[29] C.-g. Oh and S.-W. Kim, Color and transparency from quantum geometry, arXiv preprint arXiv:2507.20904 (2025).

[30] C.-g. Oh, D. Cho, S. Y. Park, and J.-W. Rhim, Bulk-interface correspondence from quantum distance in flat band systems, *Commun. Phys.* **5**, 320 (2022).

[31] H. Kim, C.-g. Oh, and J.-W. Rhim, General construction scheme for geometrically nontrivial flat band models, *Commun. Phys.* **6**, 305 (2023).

[32] T. Kitamura, A. Daido, and Y. Yanase, Spin-Triplet Superconductivity from Quantum-Geometry-Induced Ferromagnetic Fluctuation, *Phys. Rev. Lett.* **132**, 036001 (2024).

[33] F. Wu and S. Das Sarma, Quantum geometry and stability of moiré flatband ferromagnetism, *Phys. Rev. B* **102**, 165118 (2020).

[34] N. Heinsdorf, Altermagnetic instabilities from quantum geometry, *Phys. Rev. B* **111**, 174407 (2025).

[35] T. Kitamura, H. Nakai, A. Daido, and Y. Yanase, Quantum geometric ferromagnetism by singular saddle point (2025), arXiv:2505.01089 [cond-mat.str-el].

[36] K. Kudo and Y. Yanase, Odd-parity magnetism by quantum geometry (2025), arXiv:2505.20907 [cond-mat.str-el].

[37] C.-g. Oh, T. Kitamura, A. Daido, J.-W. Rhim, and Y. Yanase, Magnetic phase transitions driven by quantum geometry, arXiv preprint arXiv:2509.13618 (2025).

[38] H. Hu, O. Vafek, K. Haule, and B. A. Bernevig, Ferromagnetism vs. antiferromagnetism in narrow-band systems: Competition between quantum geometry and band dispersion (2025), arXiv:2509.03575 [cond-mat.str-el].

[39] I. I. Mazin, D. J. Singh, M. D. Johannes, and M. H. Du, Unconventional Superconductivity with a Sign Reversal in the Order Parameter of  $\text{LaFeAsO}_{1-x}\text{F}_x$ , *Phys. Rev.*

Lett. **101**, 057003 (2008).

[40] D. C. Johnston, The puzzle of high temperature superconductivity in layered iron pnictides and chalcogenides, *Advances in Physics* **59**, 803 (2010), <https://doi.org/10.1080/00018732.2010.513480>.

[41] W. Chen, Berry curvature and quantum metric in copper-substituted lead phosphate apatite, *Journal of Physics: Condensed Matter* **36**, 235601 (2024).

[42] M. M. Hirschmann and J. Mitscherling, Symmetry-enforced double Weyl points, multiband quantum geometry, and singular flat bands of doping-induced states at the Fermi level, *Phys. Rev. Mater.* **8**, 014201 (2024).

[43] K. Guo, Y. Li, and S. Jia, Ferromagnetic half levitation of LK-99-like synthetic samples, *Science China Physics, Mechanics & Astronomy* **66**, 107411 (2023).

[44] P. Wang, X. Liu, J. Ge, C. Ji, H. Ji, Y. Liu, Y. Ai, G. Ma, S. Qi, and J. Wang, Ferromagnetic and insulating behavior in both half magnetic levitation and non-levitation LK-99 like samples, *Quantum Frontiers* **2**, 10 (2023).

[45] Y. Zhang, C. Liu, X. Zhu, and H.-H. Wen, Ferromagnetism and insulating behavior with a logarithmic temperature dependence of resistivity in  $Pb_{10-x}Cu_x(PO_4)_6O$ , *Science China Physics, Mechanics & Astronomy* **67**, 217413 (2023).

[46] M. Shimizu, J. Otsuki, and H. O. Jeschke, Magnetic fluctuations in  $Pb_9Cu(PO_4)_6O$ , *Phys. Rev. B* **108**, L201105 (2023).

[47] S.-W. Kim, K. Wang, S. Chen, L. J. Conway, G. L. Pascut, I. Errea, C. J. Pickard, and B. Monserrat, On the dynamical stability of copper-doped lead apatite, *npj Comput. Mater.* **10**, 16 (2024).

[48] S.-W. Kim, K. Haule, G. L. Pascut, and B. Monserrat, Non-fermi liquid to charge-transfer mott insulator in flat bands of copper-doped lead apatite, *Mater. Horiz.* **11**, 5622 (2024).

[49] Y. Kamihara, T. Watanabe, M. Hirano, and H. Hosono, Iron-Based Layered Superconductor  $La[O_{1-x}F_x]FeAs$  ( $x = 0.05 - 0.12$ ) with  $T_c = 26$  K, *Journal of the American Chemical Society* **130**, 3296 (2008), pMID: 18293989, <https://doi.org/10.1021/ja800073m>.

[50] K. Koepernik and H. Eschrig, Full-potential nonorthogonal local-orbital minimum-basis band-structure scheme, *Phys. Rev. B* **59**, 1743 (1999).

[51] J. P. Perdew, K. Burke, and M. Ernzerhof, Generalized Gradient Approximation Made Simple, *Phys. Rev. Lett.* **77**, 3865 (1996).

[52] K. Koepernik, O. Janson, Y. Sun, and J. van den Brink, Symmetry-conserving maximally projected Wannier functions, *Phys. Rev. B* **107**, 235135 (2023).

[53] M. Tomić, H. O. Jeschke, and R. Valentí, Unfolding of electronic structure through induced representations of space groups: Application to Fe-based superconductors, *Phys. Rev. B* **90**, 195121 (2014).

[54] S. V. Krivovichev and P. C. Burns, Crystal chemistry of lead oxide phosphates: crystal structures of  $Pb_4O(PO_4)_2$ ,  $Pb_8O_5(PO_4)_2$  and  $Pb_{10}(PO_4)_6O$ , *Z. Kristallogr.* **218**, 357 (2003).

[55] L. Si and K. Held, Electronic structure of the putative room-temperature superconductor  $Pb_9Cu(PO_4)_6O$ , *Phys. Rev. B* **108**, L121110 (2023).

[56] S. Lee, J.-H. Kim, and Y.-W. Kwon, The First Room-Temperature Ambient-Pressure Superconductor (2023), arXiv:2307.12008 [cond-mat.supr-con].

[57] See Supplemental Material at URL-will-be-inserted-by-publisher for the data of the calculations.

[58] R. Thomale, C. Platt, W. Hanke, J. Hu, and B. A. Bernevig, Exotic  $d$ -wave superconducting state of strongly hole-doped  $k_xba_{1-x}fe_2as_2$ , *Phys. Rev. Lett.* **107**, 117001 (2011).

[59] F. Ma, W. Ji, J. Hu, Z.-Y. Lu, and T. Xiang, First-principles calculations of the electronic structure of tetragonal  $\alpha$ -fete and  $\alpha$ -fese crystals: Evidence for a bicolinear antiferromagnetic order, *Phys. Rev. Lett.* **102**, 177003 (2009).

[60] M. C. Lucking, F. Zheng, M. J. Han, J. Bang, and S. Zhang, Doping-induced antiferromagnetic bicolinear insulating state and superconducting temperature of monolayer fese systems, *Phys. Rev. B* **98**, 014504 (2018).